International Symposium
On Turbulence and Shear Flow
Phenomena (TSFP-9)
June 30 - July 3, 2015 *Melbourne, Australia*

BUOYANCY PROFILES INSIDE THE INNER REGION OF A CONVECTIVE BOUNDARY LAYER

Juan Pedro Mellado
Max Planck Institute for Meteorology
Bundesstr. 53, 20146 Hamburg, Germany
juan-pedro.mellado@mpimet.mpg.de

Chiel van Heerwaarden
Max Planck Institute for Meteorology
Bundesstr. 53, 20146 Hamburg, Germany
chiel.vanheerwaarden@mpimet.mpg.de

Jade Rachele Garcia
Max Planck Institute for Meteorology
Bundesstr. 53, 20146 Hamburg, Germany
jade.garcia@mpimet.mpg.de

ABSTRACT

The near-wall region in a free convective boundary layer (CBL) is investigated by means of direct numerical simulation. The CBL is forced by a constant buoyancy flux and grows into a fluid with a constant buoyancy gradient $N^2 \geq 0$. We study the dependence on N^2 of the vertical profiles of the mean and the root-mean-square (r.m.s.) of the buoyancy. We find that, although the mean buoyancy profile varies with height as $\langle b \rangle \propto z^{-1/3}$ accordingly to the classical similarity theory, the r.m.s. deviates from that theory and varies as $b_{\rm rms} \propto z^{-0.45}$. It is also found that, despite differences in the large-scale circulations induced by different values of N^2, these vertical profiles tend to become independent of N^2 near the wall. However, the depth of over which the previous scaling laws are observed increases with N^2. Spectral analysis shows that, correspondingly, the near-wall structure becomes increasingly similar among cases as the scale separation between the CBL depth and the surface scale increases.

INTRODUCTION

The free convective boundary layer (CBL) represents the planetary boundary layer in the limit of strong convective instability and weak mean horizontal wind. Under these conditions, the representation of near-wall properties in atmospheric models is often crucial because it determines the land-surface interactions and, eventually, the energy input into the system (see e.g. Wyngaard, 2010). However, the understanding of the near-wall properties in free convection remains limited. Measurements of the vertical profiles of the mean temperature, and of the variance of the temperature and velocity fluctuations, show deviations from the predictions made according to the classical similarity theory (Prandtl, 1932; Obukhov, 1946; Priestley, 1954). The reason for these deviations is attributed to the formation of large-scale circulations (LSC) that strongly affect the flow inside the near-wall region. This interaction invalidates the basic assumption made in the classical similarity theory, namely, that the near-wall region is independent of outer-layer variables (see e.g. Zilitinkevich *et al.*, 2006). A similar behavior is also observed in Rayleigh-Bénard convection (see e.g. Chillà & Schumacher, 2012).

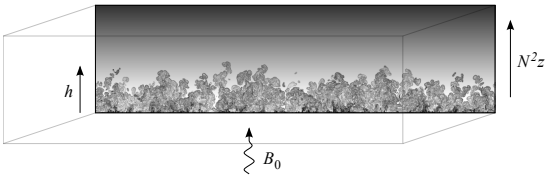

Figure 1. Sketch of the free CBL considered in this work: B_0 is the surface buoyancy flux, constant and homogeneous; N^2 is the background buoyancy gradient, constant and homogeneous (N is the buoyancy frequency, or Brunt-Väisällä frequency, inside the fluid above the CBL); h is the CBL depth, defined in equation (4).

The relevance of the large-scale circulations inside the near-wall region raises the following question: how do near-wall properties depend on outer-layer properties that can modify the large-scale circulations?

In this work, investigate the influence of the stratification inside the free troposphere. We use direct numerical simulations of a CBL over a smooth, horizontal wall that is forced by a constant surface buoyancy flux, B_0. The CBL grows into fluid with a constant buoyancy gradient, $N^2 \geq 0$ (see figure 1).

DESCRIPTION OF THE FLOW

Figure 2 illustrates the two cases considered in this work: one neutrally stratified, $N^2 = 0$, and one stably stratified, $N^2 > 0$. Regarding the vertical structure, the major difference between the two cases occurs in the entrainment zone. The entrainment zone is the upper region of the CBL where boundary-layer fluid is mixed with the fluid from the layer on top of the CBL. In the neutrally stratified case, the entrainment zone extends over a relatively large part of the CBL, and it is characterized by large-scale engulfment. In contrast, in the stably stratified case, the entrainment zone

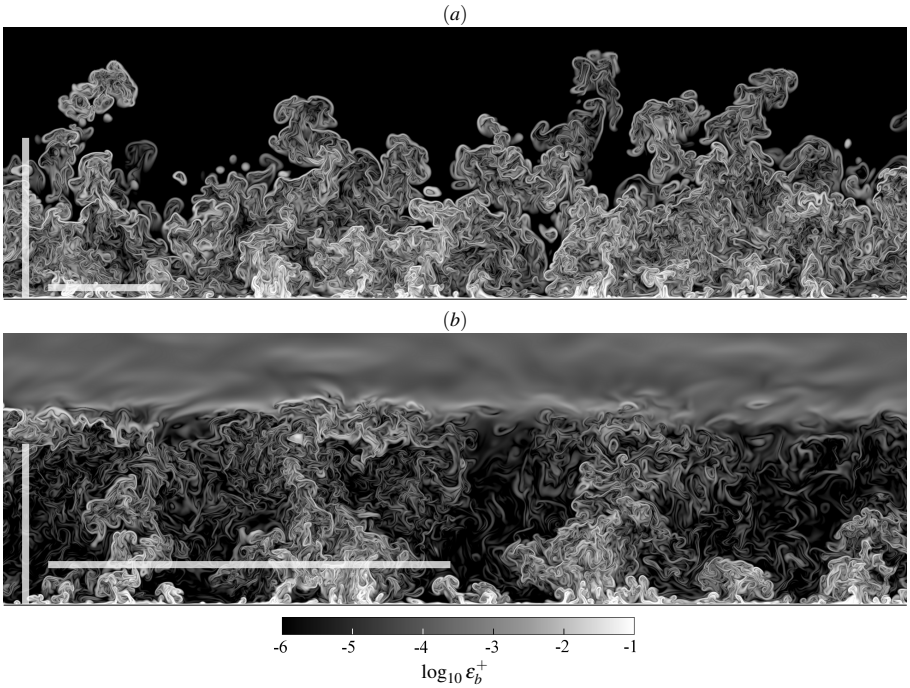

Figure 2. Vertical cross-section of the buoyancy dissipation rate $\varepsilon_b = \kappa|\nabla b|^2$ at $h^+ \simeq 680$: (a) neutrally stratified case, (b) stably stratified case. The vertical white bar in the bottom-left corner indicates the CBL depth h. The horizontal white bar is located at $z = \lambda_{\rm LSC}/10$ and extends a distance equal to $\lambda_{\rm LSC}$, the LSC size ($0.7h$ in the neutrally stratified case, $2.5h$ in the stably stratified case). Only 1/2 of the computational area is shown ($\simeq 6.1h$ in the horizontal direction).

is restricted to the upper $\simeq 20\%$ of the CBL, and the structure and dynamics of the entrainment zone depend directly on N^2 (Garcia & Mellado, 2014). Regarding the horizontal structure, the stably stratified case has wider large-scale circulations, as suggested by figure 2 and demonstrated by the spectra below.

The system is statistically homogeneous inside the horizontal planes and the statistics depend on the vertical distance from the wall, z, and the time, t. Once the details of the initial conditions have been sufficiently forgotten, the controlling parameters are $\{\nu, \kappa, B_0, N\}$, where ν is the kinematic viscosity and κ is the molecular diffusivity ($N = 0$ in the neutrally stratified configuration). Dimensional analysis shows that the statistical properties can be expressed as a function of the non-dimensional variables $\{z^+, h^+; \mathrm{Pr}, h/L_0\}$. The CBL depth h is used instead of the time to measure the evolution of the CBL, without loss of generality. The superscript "+" indicates a variable normalized by the surface scales. For an aerodynamically smooth surface, the surface length scale is

$$\delta_\kappa = (\kappa^3/B_0)^{1/4}\,, \tag{1}$$

and the corresponding velocity and buoyancy scales are

$$w_\kappa = (B_0\kappa)^{1/4}\,, \qquad b_\kappa = (B_0^3/\kappa)^{1/4}\,, \tag{2}$$

respectively (Townsend, 1959). We consider only the case of Prandtl number equal to one, i.e. $\mathrm{Pr} = \nu/\kappa = 1$.

The dependence on the stratification strength N^2 has been expressed in terms of the length scale

$$L_0 = (B_0/N^3)^{1/2}\,. \tag{3}$$

Table 1. Simulation parameters at different states of development of the CBL as indicated by h/L_0 and h^+. h is the CBL depth, L_0 the cross-over depth defined in equation (3), and h^+ is the ratio between h and the surface scale δ_κ, defined in equation (1). The convective Reynolds number Re_* is defined by equation (5).

Case	grid	h/L_0	h^+	Re_*
$N^2 > 0$	$2560^2 \times 896$	29	473	3690
	$5120^2 \times 1024$	19	679	5970
$N^2 = 0$	$5120^2 \times 860$	0	679	6970
	$5120^2 \times 1792$	0	1278	13870

This scale can be interpreted as a cross-over CBL depth beyond which N^2 influences the CBL dynamics (Garcia & Mellado, 2014). Atmospheric midday values of the ratio h/L_0 vary between 5 and 50, and a quasi-steady regime sets in at $h/L_0 \simeq 10-15$. Within this quasi-steady regime, the integral time scale of the turbulent fluctuations is much shorter than the characteristic time associated with the evolution of h, and some statistics of the flow exhibit a self-similar behavior. In the stably stratified configuration, we focus on this quasi-steady regime.

The CBL depth is defined as

$$h = \begin{cases} B_0^{-1}\int_0^\infty \langle b'w'\rangle \mathrm{d}z\,, & \text{for } N^2 = 0\,, \\ \{z : B(z) = 0\}\,, & \text{for } N^2 > 0\,, \end{cases} \tag{4}$$

where the total buoyancy flux is $B = \langle b'w' \rangle - \kappa \partial \langle b \rangle / \partial z$. Angle brackets indicate horizontal averages and apostrophes indicate fluctuation fields. Other definitions of the CBL depth are possible but they only differ in a constant of order one, so that the conclusions of this work are independent of the particular choice of h. [For instance, in the stably stratified cases, the height of minimum buoyancy flux is $1.17h$ and the height of maximum mean gradient is $1.27h$ (Garcia & Mellado, 2014).] The parameter h^+ represents the scale separation between the CBL depth, h, and the surface scale, δ_κ. It can be related to a convective Reynolds number by

$$\mathrm{Re}_* = \frac{h w_*}{\nu} = (h^+)^{4/3} \,, \tag{5}$$

where $w_* = (h B_0)^{1/3}$ is the convective velocity scale (Deardorff, 1970). Table 1 describes the values achieved in the simulations considered in this study.

BUOYANCY PROFILES

Near the wall, the mean buoyancy gradient and the r.m.s. of the buoyancy fluctuation are approximately independent of N^2, as inferred from figure 3: the vertical profiles corresponding to the two cases $N^2 = 0$ and $N^2 > 0$ approximately collapse on top of each other. This independence on N^2 implies that the near-wall structure described in Mellado (2012) for the neutrally stratified case is applicable as well to the stably stratified case: the height $10\,\delta_\kappa$ approximately marks the end of the diffusive wall layer and the beginning of the outer layer, the latter defined as the region where the molecular contribution to the total buoyancy flux is negligibly small.

The stably stratified case exhibits the clearest variation with height of the vertical profiles inside the lower part of the outer layer. The mean buoyancy gradient varies as

$$\partial \langle b \rangle^+ / \partial z^+ \simeq -0.3 (z^+)^{-4/3} \tag{6}$$

beyond $30\,\delta_\kappa$ (figure 3(a)), which agrees with the predictions that are derived from classical similarity theory (Prandtl, 1932; Obukhov, 1946; Priestley, 1954). On the other hand, the r.m.s. of the buoyancy fluctuation varies as

$$b_{\mathrm{rms}} \simeq 1.9 (z^+)^{-0.45} \tag{7}$$

(figure 3(b)), which disagrees with the prediction $b_{\mathrm{rms}} \propto (z^+)^{-1/3}$ that is derived from such a theory. This deviation indicates a dependence of near-wall properties on outer-layer variables. This deviation has been observed in other free convection systems, the exponent in the power law for b_{rms} varying within the interval $(-0.8, -0.3)$ in data from laboratory experiments (see review in Du Puits *et al.*, 2007; Mellado, 2012) and within the interval $(-1/2, -1/3)$ in data from measurements in the unstable planetary boundary layer (Wyngaard, 2010).

Regarding the dependence on N^2 inside the outer layer, the vertical profiles in the neutrally stratified case deviate from the power laws found in the stably stratified case (figure 3). The spectral analysis discussed below suggests that this deviation is caused by the large-scale circulations,

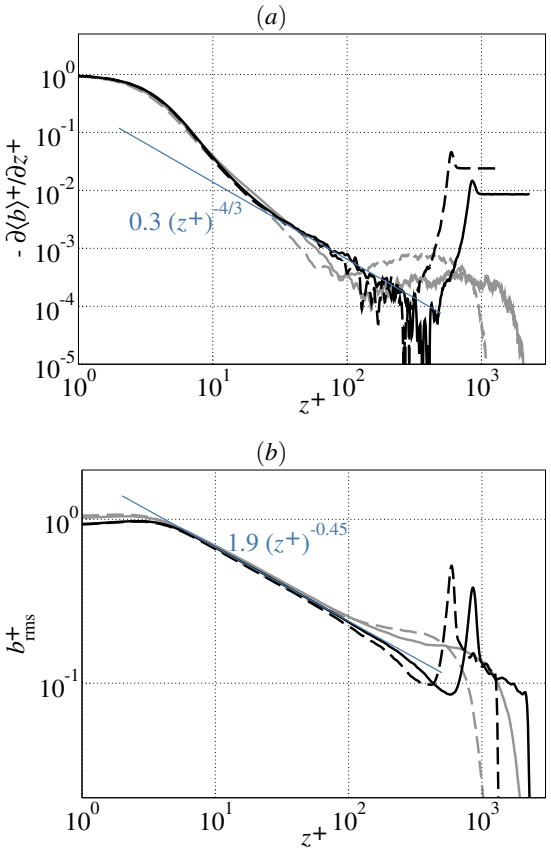

Figure 3. Vertical profiles of the magnitude of the buoyancy gradient (a), and the r.m.s of the buoyancy fluctuation (b), normalized with surface scales. Solid lines correspond to higher values of h^+, and dashed lines to lower values of h^+. Dark colors indicate the stably stratified case and light colors the neutrally stratified case.

which, for a given h^+, affect more strongly the small-scale motions near the wall when $N^2 = 0$. As the CBL thickens and h^+ increases, figure 3 indicates that the profiles in the neutrally stratified case tend towards those found in the stably stratified case. However, although we reach a relatively large value in our simulations, $h^+ \simeq 10^3$, a larger scale separation seems necessary to confirm this tendency.

SPECTRAL ANALYSIS

To better understand the near-wall region, we analyze the co-spectra between the buoyancy and the vertical velocity, and the spectra of the vertical velocity. We calculate the two-dimensional co-spectra and spectra inside each horizontal plane, integrate them azimuthally, and present them in a premultiplied form. For instance, the co-spectra is expressed as

$$\phi_{bw}(\lambda, z) \equiv (2\pi/\lambda) E^{(2)}_{bw}(2\pi/\lambda, z) \,, \tag{8}$$

where $\lambda = 2\pi/\kappa$ is the wavelength along the radial direction, so that

$$\langle b'w' \rangle = \int_0^\infty E^{(2)}_{bw}(\kappa, z) \mathrm{d}\kappa = \int_{-\infty}^\infty \phi_{bw}(\lambda, z) \mathrm{d}\log_{10}\lambda \tag{9}$$

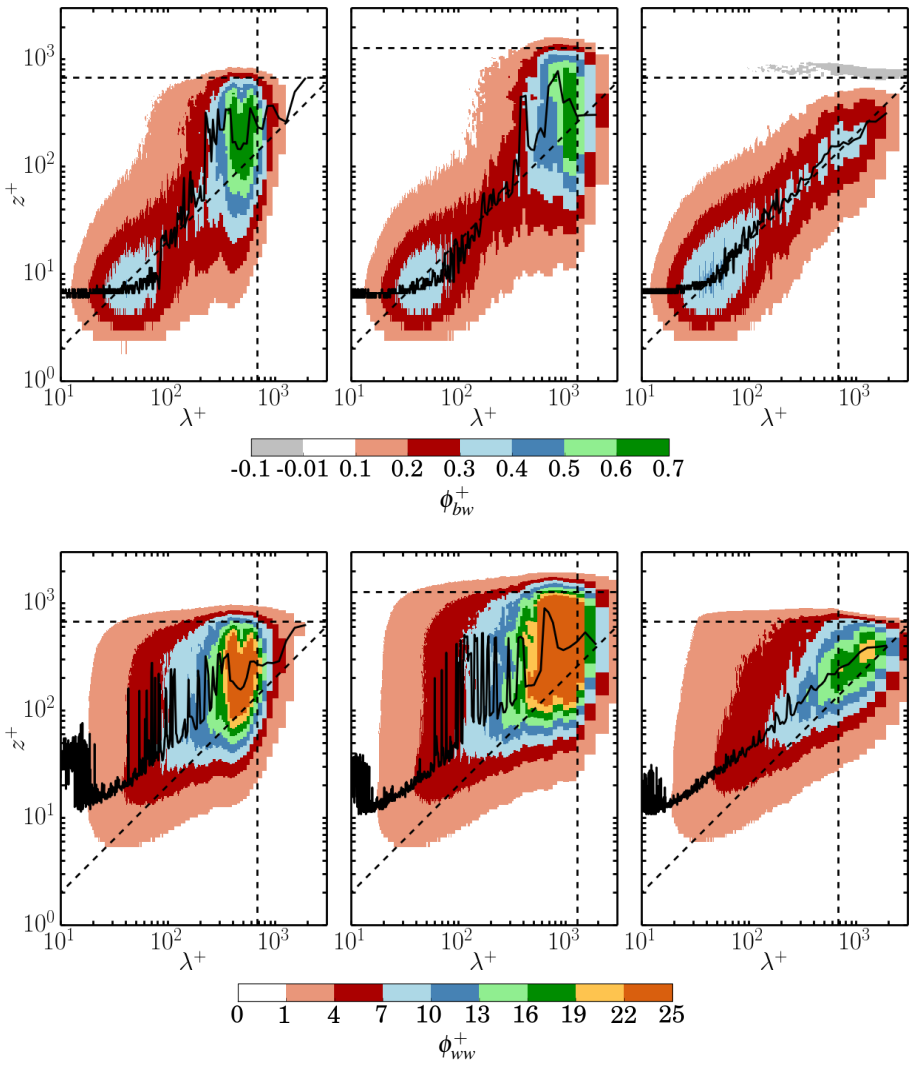

Figure 4. Premultiplied buoyancy flux co-spectra ϕ_{bw}^+ (top row) and velocity spectra ϕ_{ww}^+ (bottom row) at different states of development of the CBL: left, neutrally stratified regime at $h^+ \simeq 680$; center, neutrally stratified regime at $h^+ \simeq 1278$; right, stably stratified regime at $h^+ \simeq 680$. Solid lines mark the local spectral maxima at each wavelength. The vertical and horizontal dashed lines indicate a wavelength and a height equal to the CBL depth, h; the diagonal line corresponds to $\lambda = 5z$. [The small negative contribution in ϕ_{bw} at $z \simeq h$ and wavelengths $\simeq h$ when $N^2 > 0$ corresponds to the entrainment zone (see Garcia & Mellado, 2014) and it is not discussed here.]

holds. (The dependence on time is not shown explicitly for notational convenience.)

Near the wall, figure 4 shows that the spectral structure, when normalized with surface scales, becomes increasingly similar among cases as the scale separation between the CBL depth, h, and the surface scale, δ_κ, increases. This result has two implications. First, it further supports the use of the surface scaling for these flow properties near the wall. Second, it provides a structural definition of the inner layer.

In ϕ_{bw}, there is first a maximum at a height $z \simeq 10\,\delta_\kappa$, i.e., at the top of the diffusive wall layer. The wavelength corresponding to this maximum is $\simeq 50\,\delta_\kappa$, about 5 times that height.

Beyond $z \simeq 10\,\delta_\kappa$, inside the outer layer, most of the contribution to the turbulent buoyancy flux occurs from a bandwidth that is centered around the line

$$\lambda_{bw} = 5z \qquad (10)$$

(diagonal dashed line in figure 4). The interpretation thereof is that, as they rise, small plumes (or thermals, or both) coalesce into fewer plumes that are farther apart in the horizontal directions (Kaimal & Finnigan, 1984; Schmidt & Schumann, 1989). Here, we find that this growth is linear and well approximated by $5z$. Accordingly, the maximum of the spectra of the vertical velocity component forms along that line, slightly above as a result of the vertical advection, along the line $\lambda_{ww} = 3z$ (cf. solid lines in figure 4). The magnitude of this maximum increases with height as the plumes and thermals accelerate. The linear increase with height of the dominant wavelength of ϕ_{ww} agrees as well with that observed in the planetary boundary layer (Kaimal & Finnigan, 1984; Wyngaard, 2010).

In contrast to the near-wall structure, the outer-layer structure is strongly influenced by the stratification. On the one hand, in the stably stratified cases, plume coalescence continues until a height at which the dominant wavelength

λ_{bw} becomes slightly larger than the CBL depth (top row in figure 4). On the other hand, plume coalescence ends earlier in the neutrally stratified case, and a second, stronger maximum in the co-spectrum ϕ_{bw} appears at smaller wavelengths, at $\simeq 0.7h$.

The maxima of ϕ_{ww} form at those locations and at those wavelengths where plume coalescence ends. As inferred from figure 4 (bottom row), the wavelengths of these maxima, λ_{LSC}, are proportional to the CBL depth. The magnitudes of these maxima are proportional to the maximum w_{rms} and thus proportional to the outer velocity scale $w_* = (hB_0)^{1/3}$ (not shown). Therefore, we associate these maxima of ϕ_{ww} with large-scale circulations, a form of large-scale motion that is characteristic of free convection (see e.g. Stull, 1988; Chillà & Schumacher, 2012).

To estimate the LSC geometry, we notice that the maximum of ϕ_{ww} occurs at a height $\simeq 0.5h$. Using the relation $\lambda_{bw} = 5z$ to relate heights and wavelengths, the corresponding LSC size is $\lambda_{\mathrm{LSC}} = 5 \times 0.5h = 2.5h$. In the neutrally stratified case, plume coalescence ends closer to the wall. We approximate the final height by $0.7h/5 = 0.14h$, so that $\lambda_{\mathrm{LSC}} \simeq 0.7h$ when $N^2 = 0$, which is the wavelength of the outer-layer maximum observed before in ϕ_{bw} and ϕ_{ww}. The large-scale patterns visualized in figure 2 support these length-scale definitions.

Last, we note that the depth of the inner region over which the scaling laws reported in the previous section are valid (cf. figure 3) is well approximated by $\lambda_{\mathrm{LSC}}/10$, in all cases. For $h^+ \simeq 680$, this means $\simeq 50\,\delta_\kappa$ in the neutrally stratified configuration and $\simeq 170\,\delta_\kappa$ in the stably stratified configuration; for $h^+ \simeq 1280$, this means $\simeq 90\,\delta_\kappa$ in the neutrally stratified configuration. This result implies that, for a given h, the inner region in the strong stratification regime penetrates deeper into the outer layer, and its depth is $\simeq 4$ times larger than in the weak stratification regime and $\simeq 2.5$ times larger than the thickness $\simeq 0.1h$ commonly used to define a constant-flux (or surface) layer (see e.g. Wyngaard, 2010).

CONCLUSIONS

There are two main results. First, the vertical profiles of the buoyancy field near the wall show deviations from the predictions made according to the classical similarity theory: whereas the mean buoyancy gradient varies as $z^{-4/3}$ with respect to the distance to the wall, z, the r.m.s of the buoyancy fluctuation varies as $z^{-0.45}$, instead of $z^{-1/3}$. This behavior is consistent with measurements from the unstable planetary boundary layer (see e.g. Zilitinkevich *et al.*, 2006), and also with analysis from Rayleigh-Bénard convection (see e.g. Chillà & Schumacher, 2012).

Second, near the wall, the vertical profiles are approximately independent of the stratification of the fluid above the CBL, N^2, and they follow surface scaling. However, the vertical extent over which the previous scaling laws are observed depends on N^2. The same behavior is observed in the spectra of the buoyancy flux and the vertical velocity. This result can be interpreted as a dependence of the inner-layer depth on N^2: For a given CBL depth, h, the inner-layer depth in the stably stratified is $\simeq 0.25h$ more than three times the value in the neutrally stratified case.

There are two possible physical explanations for this second result. First, the entrainment zone in the neutrally stratified case penetrates deeper inside the CBL, modifying thereby the flow structure closer to the wall. Second, the horizontal velocity intensifies with increasing stratification, in particular in the lower CBL half (not shown). This intensification demands an acceleration and coalescence of ascending plumes for a longer time until they acquire a vertical velocity comparable to the horizontal one, so that they an escape the coalescence process—a longer acceleration time means longer distances, which implies a deeper region of plume coalescence.

REFERENCES

Chillà, F. & Schumacher, J. 2012 New perspectives in turbulent Rayleigh-Bénard convection. *Eur. Phys. J. E* **35** (58), 1–25.

Deardorff, J. W. 1970 Convective velocity and temperature scales for the unstable planetary boundary layer and for Rayleigh convection. *J. Atmos. Sci.* **27**, 1211–1213.

Garcia, J. R. & Mellado, J. P. 2014 The two-layer structure of the entrainment zone in the convective boundary layer. *J. Atmos. Sci.* **71**, 1935–1955.

Kaimal, J. C. & Finnigan, J. J. 1984 *Atmospheric Boundary Layer Flows*. Oxford University Press.

Mellado, J. P. 2012 Direct numerical simulation of free convection over a heated plate. *J. Fluid Mech.* **712**, 418–450.

Obukhov, A. M. 1946 Turbulence in an atmosphere with a non-uniform temperature. *Tr. Inst. Teo. Geofiz. Akad. Nauk. SSSR* **1**, 95–115, in Russian, English trans.: 1971 *Boundary-Layer Meteorol.* **2**, 7–29.

Prandtl, L. 1932 Meteorologische Anwendung der Strömungslehre. *Beitr. Phys. Atmos.* **19**, 188–202.

Priestley, C. H. B. 1954 Convection from a large horizontal surface. *Austr. J. Phys.* **7**, 176–201.

Du Puits, R., Resagk, C., Tilgner, A., Busse, F. H. & Thess, A. 2007 Structure of thermal boundary layers in turbulent Rayleigh-Bénard convection. *J. Fluid Mech.* **572**, 231–254.

Schmidt, H. & Schumann, U. 1989 Coherent structure of the convective boundary layer derived from large-eddy simulations. *J. Fluid Mech.* **200**, 511–562.

Stull, R. B. 1988 *An Introduction to Boundary Layer Meteorology*. Kluwer Academic Publishers.

Townsend, A. A. 1959 Temperature fluctuations over a heated horizontal surface. *J. Fluid Mech.* **5**, 209–241.

Wyngaard, J. C. 2010 *Turbulence in the Atmosphere*. Cambridge University Press.

Zilitinkevich, S. S., Hunt, J. C. R., Esau, I. N., Grachev, A. A., Lalas, D. P., Akylas, E., Tombrou, M., Fairall, C. W., Fernando, H. J. S., Baklanov, A. A. & Joffre, S. M. 2006 The influence of large convective eddies on the surface-layer turbulence. *Q. J. Roy. Meteorol. Soc.* **132**, 1423–1455.